Dependence of the binary-encounter-peak energy on the projectile core

J. M. Sanders,* J. L. Shinpaugh,† and S. Datz
Physics Division, Oak Ridge National Laboratory, Oak Ridge, Tennessee 37831

F. Segner and M. Breinig
Department of Physics, University of Tennessee, Knoxville, Tennessee 37996
and Physics Division, Oak Ridge National Laboratory, Oak Ridge, Tennessee 37831
(Received 13 December 1995; revised manuscript received 26 September 1996)

The energy of the binary-encounter peak has been determined for 0.6 MeV/u O, F, Si, Ti, Cu, and Br ions colliding with H_2 targets. The projectiles all had the same charge $q=7$, while the atomic number Z of the projectiles ranged from 8 (almost totally ionized) to 35 (retaining 28 electrons). We observe that the binary-encounter-peak energy for fixed q increases as Z increases. This trend is opposite to that observed when Z is fixed and the charge q is varied, and it demonstrates that the binary-encounter-peak energy depends not only on the net projectile charge but on the projectile core as well. The experimental trend is qualitatively reproduced by an impulse approximation showing that this variation in the binary-encounter-peak energy may be attributed to the effect that the projectile core potential has on the electron elastic-scattering cross section. [S1050-2947(97)07001-7]

PACS number(s): 34.50.Fa

I. INTRODUCTION

The binary-encounter peak is a prominent feature of the spectrum of fast electrons produced at forward angles in collisions of highly charged ions with target atoms [1]. The peak is termed ''binary encounter,'' because it has been possible to explain many of its features by considering interactions between only two bodies: the scattered target electron and the projectile ion.

The simplest approach for describing the binary-encounter mechanism is the elastic-scattering model (also known as the impulse approximation) [2–4]. It treats the collision as elastic scattering of the target electron in the projectile rest frame, and it includes the velocity distribution due to the motion of the target electrons about the target nucleus. In this model, the double-differential cross section, in the projectile rest frame, for ionizing the target is obtained from a product of the Compton profile $J(p_z)$ of the target electrons and the elastic-scattering cross section $\sigma_{\rm el}$ by

$$\frac{d^2\sigma}{dE\,d\Omega}=\frac{d\sigma_{\rm el}}{d\Omega}\frac{J(p_z)}{(V_p+p_z)}. \tag{1}$$

The momentum distribution of the electrons on the target atom is given by the Compton profile

$$J(p_z)=\int\int dp_x dp_y|\psi(\mathbf{p})|^2, \tag{2}$$

where $\psi(\mathbf{p})$ is the electron momentum wave function. The component p_z of the electron momentum about the target nucleus in the direction of the projectile velocity V_p is given by

$$p_z=\sqrt{2m_e(E+E_b)}-m_eV_p, \tag{3}$$

where E is the electron kinetic energy in the projectile frame, E_b is the binding energy of the electron on the target atom, and m_e is the electron mass.

Several studies of the energy of the binary-encounter peak have been performed, and it has been observed that the binary-encounter peak occurs at an energy lower than the energy expected for a collision of the projectile with a free electron at rest [4–13]. To quantify the difference between the experimental binary-encounter peak and the energy for the scattering of a free electron initially at rest, the energy shift

$$\Delta E=2m_eV_p^2-E_{\rm BEP} \tag{4}$$

is defined where m_e is the mass of the electron, V_p is the projectile velocity, and $E_{\rm BEP}$ is the energy of the maximum of the binary-encounter peak measured in the laboratory rest frame [4]. This definition has the advantage of consisting of experimentally determined quantities and is independent of any particular theoretical treatment of the ionization process.

The elastic-scattering model of Eqs. (1)–(3) has been employed to identify two contributions to this energy difference. The first effect is that the symmetric Compton profile is skewed toward lower energies by the energy dependence of the elastic scattering cross section [4]. This is demonstrated in Fig. 1. In the figure, the dashed curve shows $d\sigma_{\rm el}/d\Omega$ alone. The dotted curve shows $J(p_z)$ alone. The solid curve is the full result of Eq. (1). It can be seen that the elastic scattering cross section weights the low-energy side of the Compton term more heavily than the high-energy side, resulting in a total curve that maximizes at a lower energy than

*Present address: Department of Physics, University of South Alabama, Mobile, AL 36688.
†Present address: Department of Physics, East Carolina University, Greenville, NC 27858.

 © 1997 The American Physical Society

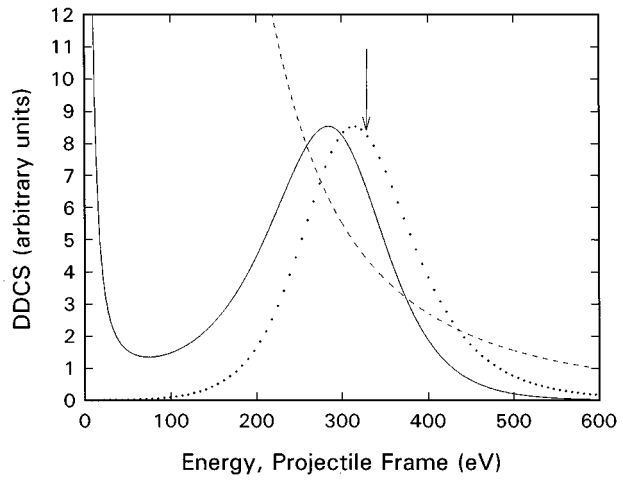

FIG. 1. Contributions of the binary-encounter-peak energy shift in the elastic-scattering model. The dotted curve, emphasizing the role of the binding energy of the target, shows a Compton profile evaluated using Eq. (3). The dashed curve shows the elastic-scattering cross section. The solid curve shows the product of the two previous curves, emphasizing the role played by the elastic-scattering cross section in shifting the binary-encounter peak toward lower energies.

the Compton term alone. The second contribution to the shift in the elastic-scattering model is the target electron binding energy [4,5] which enters directly into Eq. (3).

The elastic-scattering model discussed above initially appeared to predict the energy shift of the binary-encounter peak rather well. Lee *et al.* found that for 1.5-MeV/u bare C, N, O, and F projectiles, the model only slightly underestimated the shift [4]. However, when projectiles with much different charges were used, differences between the elastic-scattering model and experiment were seen. The model predicts that all bare projectiles should have the same shift, since all have the same energy dependence for the elastic scattering cross section $(1/E^2)$. Lee *et al.* did not observe such an independence of projectile charge; their measured shift for 1.5-MeV/u H^+ was much smaller than for the other bare projectiles with charges between 6 and 9 [4]. Several subsequent experiments have amply demonstrated that the shift of the binary-encounter-peak energy does, in fact, depend on the net projectile charge q [6–13], which for bare ions is Z.

Pedersen *et al.* [7] proposed a model, based upon the Bohr-Lindhard model for ionization, which provided an explanation for the dependence on projectile charge. A similar argument for the q dependence of the energy shift was provided by Fainstein, Ponce, and Rivarola [14]. In these models, the ionized electron must lose some of its kinetic energy in order to escape from the potential well of the projectile. Both models predict that ΔE should vary as $\sqrt{q}$ for pure Coulomb projectile potentials. In both models, the ionization process is considered to occur at some ''ionization radius'' from the projectile nucleus. For loosely bound target electrons, the ionization radii used by both models are typically several atomic units in length, so for nonbare projectiles, the potential used to calculate the energy shift is evaluated where the projectile nuclear charge is fully screened by the projectile electrons. These models, in short, are insensitive to the projectile potential near the nucleus and predict that the energy of the binary-encounter peak should change only as a function of the net projectile charge.

Experimental tests of both the Pedersen and Fainstein models have indicated that the models can approximately predict the q dependence of the binary-encounter-peak energy shift, but the experiments to date have not verified that the shift depends solely on the net projectile charge. Hidmi *et al.* [10] found that Pedersen's model was successful in predicting ΔE for 0.5-Mev/u Cu^{q+} projectiles, but the agreement with the data became progressively worse for lower Z projectiles. This result suggests that ΔE may be a function of projectile Z as well as of the net projectile charge q. Wolff *et al.* [11] found that ΔE given by Fainstein's model agreed well with their measured shifts for a variety of heavy 0.6-MeV/u projectiles. They concluded, on the basis of the apparent success of the Fainstein model applied to nonbare projectiles, that the binary-encounter-peak shift depended solely on q and not on Z. However, since both q and Z were varied simultaneously in that experiment, agreement with the purely q-dependent models does not constitute clear proof that there is no Z dependence.

The goal of this experiment was to determine whether the binary-encounter-peak energy shift depends on the projectile core potential. To achieve this goal, Z was the only parameter allowed to vary: both the projectile velocity and the projectile charge were held fixed at 0.6 MeV/u and 7+ respectively. By holding q fixed while varying Z, the projectile potential was changed from one that was nearly pure Coulomb to one that deviated greatly from Coulomb.

II. THEORY

The simple elastic-scattering model given above in Eqs. (1)–(3) is a somewhat crude implementation of the impulse approximation. Its main result [Eq. (1)] is useful in seeing qualitatively the effects of changing the variables of the collision. For more quantitative analysis, a more rigorous impulse approximation calculation must be performed. In analyzing the present results, we have used an implementation of the impulse approximation following the notation used in Wang, Reinhold, and Burgdörfer [15].

Let $\mathbf{k}_f$ be the momentum of the electron in the projectile frame after scattering. Let ϵ_i be the binding energy of the electron in the target before scattering. Let $\tilde{\varphi}_i(\mathbf{p})$ be the momentum-space representation of the electron wave function in the initial state. Finally, let T_{fi} be the two-body transition matrix element. Then the double-differential cross section (in a.u.) in the impulse approximation is given by

$$\frac{d^2\sigma}{dE_f d\Omega_f} = \frac{16\pi^4}{v} \int d^3q\, \delta\left(\mathbf{q}\cdot\mathbf{v} - \frac{k_f^2 + v^2 - 2\epsilon_i}{2}\right) \times |T_{fi}(\mathbf{k}_f, \mathbf{q})\tilde{\varphi}_i(\mathbf{q}-\mathbf{v})|^2. \quad (5)$$

The T matrix element in Eq. (5) is the exact off-shell element, and there are various frequently employed on-shell approximations to it. We use the second on-shell approximation discussed by Wang, Reinhold, and Burgdörfer, very similar to the elastic scattering model of Burch, Wieman, and Ingalls [16], and we refer to it hereafter as OSA2.

The on-shell approximation employed in this paper (OSA2) sets

$$\frac{16\pi^4}{v}\, q_0 |T_{fi}(\mathbf{k}_f,\mathbf{q})|^2 \equiv \sigma_{\rm el}\left(\frac{q_0^2}{2},\cos\theta_{\rm eff}\right), \tag{6}$$

where $\sigma_{\rm el}$ is the electron elastic-scattering cross section, and the effective scattering angle $\theta_{\rm eff}$ is given by

$$\cos\ \theta_{\rm eff} = 1 - |\mathbf{q}_0 - \mathbf{k}_f|^2/2q_0^2. \tag{7}$$

Then Eq. (5) becomes

$$\frac{d^2\sigma}{dE_f d\Omega_f} = k_f \int d\Omega_{q_0} \sigma_{\rm el}\left(\frac{q_0^2}{2},\cos\theta_{\rm eff}\right) |\tilde{\varphi}_i(\mathbf{q}_0 - \mathbf{v})|^2. \tag{8}$$

The differential elastic-scattering cross sections $\sigma(E,\theta)$ for free electrons scattering from the projectile potentials were calculated using the partial-wave method. The spherically symmetric scattering potentials employed were the exact analytical forms in the case of bare and one-electron ions, and Hartree-Fock potentials were used for the multielectron ions.

The momentum-space probability density $|\tilde{\varphi}_i(\mathbf{p})|^2$ of the electron in its initial state on the target hydrogen molecule was obtained from the experimental Compton profile of H_2. If the spherically averaged momentum probability density is assumed to be spherically symmetric, then

$$|\tilde{\varphi}_i(\mathbf{p})|^2 = \frac{1}{4\pi} |\chi(p)|^2, \tag{9}$$

where $\chi(p)$ is the radial part of the momentum-space wave function. The expression for the Compton profile can be written

$$J(p_z) = \int\int |\tilde{\varphi}_i(\mathbf{p})|^2 dp_x dp_y = \frac{1}{2}\int_{p_z}^{\infty} |\chi(p)|^2 p\ dp. \tag{10}$$

Thus $|\chi(p)|^2$ will be given by differentiating Eq. (10) by p_z, and the momentum-space probability density results from

$$|\tilde{\varphi}_i(\mathbf{p})|^2 = \frac{1}{4\pi} |\chi(p)|^2 = -\frac{1}{2\pi p_z}\frac{dJ(p_z)}{dp_z}. \tag{11}$$

To evaluate Eq. (11), Lee's empirical expression for the Compton profile of H_2 was employed [17]. With the momentum-space probability density given by Eq. (11), the integral in Eq. (8) could be evaluated to yield the OSA2 cross section. Results of such a calculation will be discussed in Sec. V.

III. EXPERIMENT

This experiment was performed at the ORNL EN Tandem Van de Graaff Facility. Beams of 0.6-MeV/u ions were extracted from the accelerator, and, for some beams, the desired charge state was obtained by passing the beam through a 5-μg/cm^2 carbon foil. After magnetic charge-state selection, the ion beam was then collimated by passing it through two 0.75-mm-diam apertures separated by 1.32 m. A third aperture 1 mm in diameter and located 10 cm downstream skimmed off ions scattered at the edges of the two upstream apertures. The spectrometer was located approximately 33 cm from the third aperture. After passing through the gas cell and spectrometer, the beam was collected in a Faraday cup located 2 m downstream.

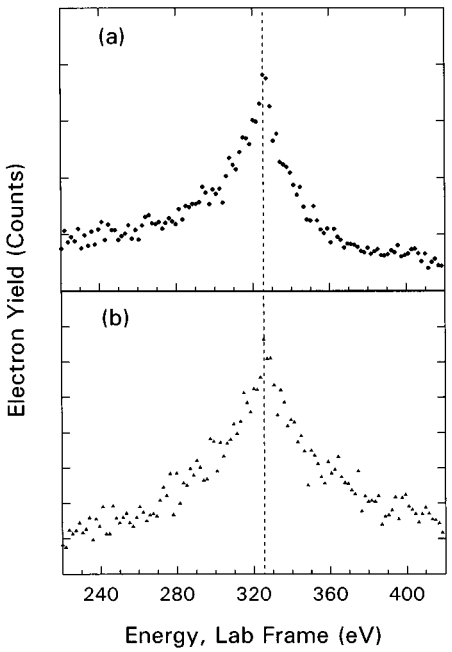

FIG. 2. Comparison of the cusp spectra for (a) 0.6-MeV/u F^{7+} projectiles incident on H_2 and (b) 0.6-MeV/u Br^{7+} projectiles incident on Ar. The vertical dashed line indicates the peak maxima.

The target gas cell was 1.2 cm long with an entrance aperture 1.4 mm in diameter and an exit aperture 1.7 mm in diameter. The typical H_2 target gas pressure in the gas cell was 20 mTorr. Hydrogen was chosen as the target gas because its Compton profile (hence the binary-encounter peak) is narrow showing a sharp maximum, and its Compton profile has been accurately measured [17].

The spectrometer was placed to observe the electrons emitted at 0° with respect to the beam direction. The spectrometer was an electrostatic spherical-sector analyzer with a central-ray radius of 5.47 cm. Its energy resolution was 2%, and its angular acceptance was 1.6°. Electrons analyzed by the spectrometer were detected with a channel electron multiplier. The dwell time at each spectrometer voltage was determined by the integrated beam collected in the Faraday cup.

For each ion beam, two electron spectra were taken. One spectrum concentrated on the cusp and was taken with a 1.8-eV step size. The cusp spectrum was used to determine the velocity of the beam as described in the following section. Argon was used as the target gas rather than H_2 in obtaining some of the cusp spectra, since Ar provided a more prominent cusp, and the substitution did not otherwise affect the determination of the beam velocity. The second spectrum, always taken with a H_2 target, covered both the cusp and the binary-encounter peak and was taken with 7.1-eV step size. Examples of cusp spectra are given in Fig. 2, while a full spectrum is shown in Fig. 3.

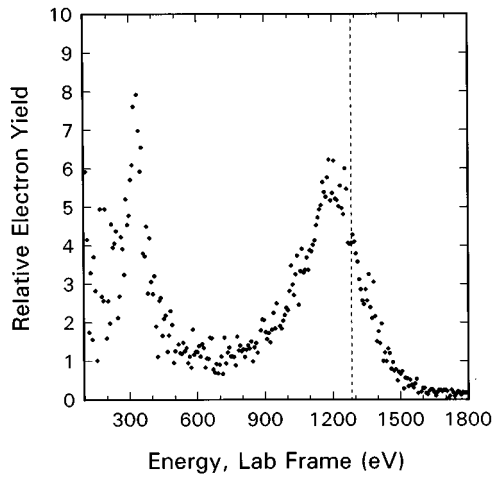

FIG. 3. A spectrum for the full energy range examined in this experiment showing the cusp and the binary-encounter peak for 0.6-MeV/u Br^{7+} on H_2. The dashed line marks the energy that would result from a collision of the projectile with a free electron at rest.

IV. DATA ANALYSIS

Electron spectra, obtained as described above, were fitted using nonlinear least-squares fitting routines to determine the quantities of interest. The cusp spectrum was fitted to determine the beam velocity V_p, and the binary-encounter spectrum was fitted to determine the energy of the binary-encounter peak E_{BEP}. With these two quantities, the binary-encounter-peak energy shift ΔE could be calculated using Eq. (4). Further details of the fitting procedures are given next.

A. Determination of projectile velocity

Using the energy of the electron cusp peak has been a convenient method of determining projectile velocities [4,8,10,18], since the cusp electrons have roughly the same velocity as the projectile. The technique is useful when the energy of the beam is not well known, for example, due to energy loss in passing through a foil. However, it is necessary to take some care in extracting a projectile velocity from a cusp spectrum. The electron cusp is formed primarily by electron loss to the continuum (ELC) and electron capture to the continuum (ECC). Comparing the cusps for F^{7+} and Br^{7+} shown in Fig. 2, it can be seen that the cusp for F^{7+} is skewed slightly to the low-energy side, while the Br^{7+} cusp is more symmetric. This skewing of the F^{7+} cusp is an example of the well-known asymmetry of ECC cusps [19]. Br^{7+} has a greater contribution from ELC which produces a more symmetric cusp. Since the cusps are generally asymmetric, neither the cusp maximum nor the centroid are accurate measures of the beam velocity.

In order to accurately determine the projectile velocity from a cusp spectrum, an empirical line shape was fitted to the cusp using nonlinear least-squares fitting routines [20]. The line shape was given by the multipole expansion of Meckbach, Nemirovsky, and Garibotti [21]. The differential cross section was expanded as a power series in the electron velocity $\mathbf{v}'$ in the projectile frame and in Legendre polynomials of the emission angle $\cos\theta' = \hat{\mathbf{v}}' \cdot \hat{\mathbf{V}}_p$:

$$\frac{d\sigma}{d\mathbf{v}'} = \frac{1}{v'} \sum_{n=0}^{\infty} \sum_{l=0}^{\infty} (v')^n B_{nl} P_l(\cos\theta'). \tag{12}$$

This expansion was convoluted with the spectrometer function $S(v,\Omega)$ to give an electron yield

$$Y(v,\theta) = \sum_{n=0}^{\infty} \sum_{l=0}^{\infty} B_{nl} Q_{nl}(v,\theta), \tag{13}$$

where the functions $Q_{nl}(v,\theta)$ are given by

$$Q_{nl}(v,\theta) = \int_v \int_\Omega v^2 (v')^{n-1} P_l(\cos\theta') S(v,\Omega)\, dv\, d\Omega. \tag{14}$$

The spectrometer function $S(v,\Omega)$ was given by

$$S(v,\Omega) = \begin{cases} 1 & \text{if } 0 \leqslant \theta \leqslant \theta_0 \text{ and } v_0 - \Delta v \leqslant v \leqslant v_0 + \Delta v \\ 0 & \text{otherwise.} \end{cases} \tag{15}$$

For the spectrometer used in this experiment, the angular acceptance θ_0 was 1.6° and the velocity resolution $\Delta v/v_0$ was 0.5%.

Only the first few terms ($n \leqslant 1$ and $l \leqslant 2$) in the sum in Eq. (13) were required to obtain good fits to the experimental electron yields. The coefficients B_{nl} and the projectile velocity V_p were the parameters extracted from the least-squares fit of Eq. (13) to the data.

In the present experiment, it was possible, for some of the projectile beams, to either obtain a beam of the desired charge state directly from the accelerator or to compensate for the energy loss in the carbon foil used to change the charge of the beam. For these beams, a projectile velocity could be measured by magnetic analysis to within 1%. Since projectile velocities obtained using the above fitting procedure agreed well with the velocities determined by magnetic analysis for those beams where magnetic analysis could be employed, the cusp method was used to determine the velocities of the remaining beams.

B. Determination of binary-encounter-peak energy

To obtain the binary-encounter-peak energy, the electron spectrum was fitted with an empirical function based on the elastic-scattering model given by Eqs. (1) and (3). For the elastic-scattering cross section, the Rutherford scattering cross section, appropriate for a pure Coulomb potential, was used. Inserting the Rutherford cross section for 180° scattering into Eq. (1) yielded the fitting function [4]:

$$f(E) = A\, \frac{J(p_z)}{E^2 \sqrt{E + E_b}}, \tag{16}$$

where p_z was given by Eq. (3) and the Compton profile $J(p_z)$ for H_2 was the analytic form given by Lee [17]. The multiplicative normalization constant A and the ''binding energy'' E_b were allowed to vary in order to obtain the least-squares fit. This empirical profile has been found to model the shape of binary-encounter peaks very well. An example

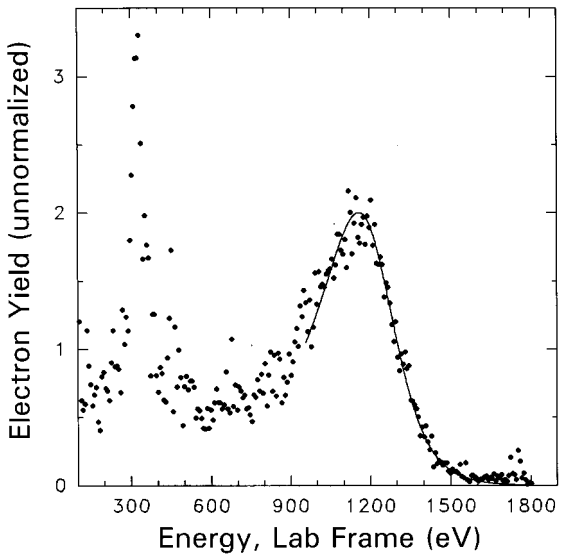

FIG. 4. Result of a least-squares fit to the binary-encounter peak. The data are for 0.6-MeV/u Cl^{7+} on H_2. The solid line shows the result of the least-squares fit.

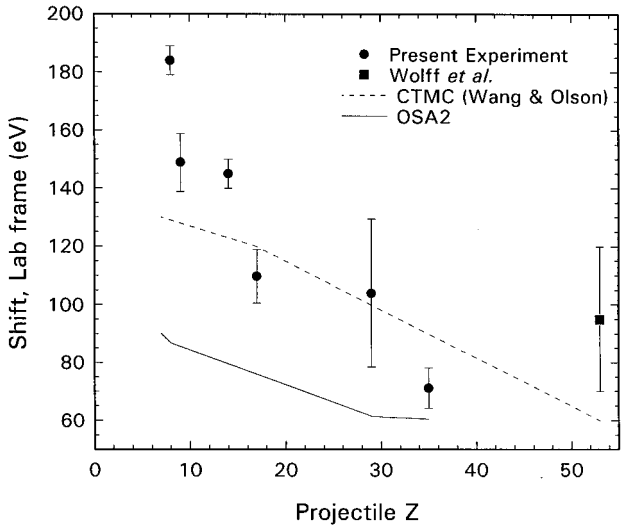

FIG. 5. Shift of the binary-encounter-peak energy plotted versus the projectile atomic number. The projectiles have the same squared velocity 0.6 MeV/u and charge 7. The circles are the shifts measured in the present experiment, the square is a shift measured by Ref. [11]. The solid curve is the OSA2 impulse approximation calculation described in Sec. II. The dashed curve is the classical trajectory Monte Carlo calculation from Ref. [22].

of such a fit is shown in Fig. 4. Once the best-fit curve was determined, its maximum was computed, and the energy of this maximum was taken as the binary-encounter-peak energy E_{BEP} for use in computing shifts with Eq. (4).

C. Analysis of uncertainties

The uncertainty in the binary-encounter-peak shift δE can be obtained from Eq. (4) by usual propagation of errors:

$$\delta E=\left[\left(\frac{\partial(\Delta E)}{\partial V_p}\,\Delta V_p\right)^2+\left(\frac{\partial(\Delta E)}{\partial E_{\mathrm{BEP}}}\,\Delta E_{\mathrm{BEP}}\right)^2\right]^{1/2}. \quad (17)$$

To evaluate this expression, it is necessary to find the uncertainty in the projectile velocity ΔV_p and the uncertainty in the binary-encounter-peak energy ΔE_{BEP}.

The fitting procedures discussed above yielded the projectile velocity and the binary-encounter-peak energy. The statistical uncertainties in the fitted parameters were given by the diagonal elements of the error matrix produced in the least-squares fit [20], so ΔV_p was obtained from the error matrix when the cusp spectrum was fitted. E_{BEP} was not itself a parameter of the fit to the binary-encounter spectrum, but was computed from the fitted profile as discussed above. Thus ΔE_{BEP} had to be obtained by numerically determining the variation in E_{BEP} arising from variations in the fitting parameters A and E_b and also from V_p, since it indirectly enters into the computation of the fitting profile through p_z. In this fashion, the statistical uncertainties in the projectile velocity and in the binary-encounter-peak energy, ΔV_p and ΔE_{BEP}, were obtained. The statistical uncertainty of the binary-encounter-peak energy shift was then computed using Eq. (17).

In addition to the statistical uncertainty in the various fitted parameters, there were also systematic uncertainties. One source of error was in small differences in the alignment of the spectrometer and beam over the course of data taking. That is, the beam might wander slightly in its trajectory down the beamline during the time that a spectrum was being taken or between the time that the cusp spectrum was taken and the full spectrum was taken. These differences in alignment would require the beams to have slightly different trajectories through the analyzing magnet, and therefore the beams would have slightly different energies. This component of the error was difficult to quantify *a priori*, so a direct measurement of this variation was required. For each beam, spectra were taken on more than one occasion, and the average and standard deviation of the shifts from these spectra, weighted by their statistical uncertainties, were computed. This standard deviation was then added in quadrature with the statistical uncertainties from the fitting procedures. The result was taken to be the total uncertainty in the energy shift of the peak and is shown as the error bars in Fig. 5. The systematic errors, as measured by the standard deviation of the mean for the several spectra, generally made a far larger contribution to the total error than did the statistical uncertainties from the fitting procedures.

V. RESULTS AND CONCLUSIONS

The shifts in the binary-encounter-peak energy are plotted in Fig. 5. A decrease of about a factor of 2 is observed as the projectile Z is increased from 8 to 35. Also plotted in the figure is the energy shift from Ref. [11] for an iodine ($Z=53$) projectile at the same velocity and charge used in this experiment. The data clearly show that the shift of the binary-encounter-peak energy depends on the projectile core independent of the net charge of the projectile ion.

Also in Fig. 5 are two theoretical calculations: the OSA2 impulse approximation discussed in Sec. II above, and classical-trajectory Monte Carlo (CTMC) calculations provided by Wang and Olson [22]. Both calculations agree qualitatively with the data, although the OSA2 considerably

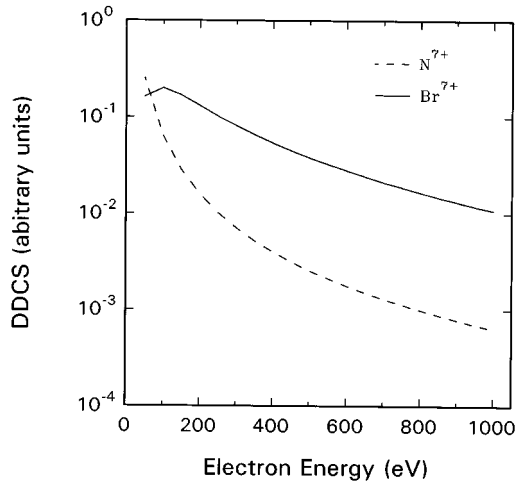

FIG. 6. Comparison of the cross sections for elastic scattering of electrons from N^{7+} and Br^{7+} calculated using the partial-wave method.

underestimates the magnitude of the shift. The decrease of binary-encounter-peak energy shift seen in Fig. 5 can also be explained qualitatively by the simple elastic scattering model of Eqs. (1)–(3). In that model, part of the shift is a result of the energy dependence of the elastic-scattering cross section. The shift is large when the elastic-scattering cross section is a rapidly varying function of energy—a steep slope for the elastic-scattering cross section implies a large shift. In Fig. 6 are shown the elastic cross sections for scattering at 180° degrees for electrons colliding with N^{7+} and Br^{7+}. The elastic-scattering cross section decreases more steeply for N^{7+} than for Br^{7+} in the projectile frame energy range of 329 eV; therefore the energy shift is expected to be greater for N^{7+} than for Br^{7+}.

These results show that the binary-encounter-peak energy shift depends on the projectile core in addition to its dependence on net q. Furthermore, while ΔE *increases* with increasing q, it *decreases* with increasing Z. This trend is predicted by neither the Pedersen nor Fainstein model even when non-Coulomb potentials are used in the latter. In both of these models, the shift is related to the projectile potential at large distances from the projectile nucleus where the nuclear charge is essentially fully screened, so no core effects are expected in these models. These results also show that the binary-encounter-peak energy is shifted by different projectile cores, because the core potentials give rise to elastic-scattering cross sections that have differing energy dependences.

A secondary conclusion of this work is that the shift of binary-encounter-peak energy calculated using Eq. (4) is very sensitive to the error made in determining the projectile velocity. Great care must be exercised in deriving beam velocities from the electron cusp. Therefore simply taking the cusp maximum or centroid is insufficient for asymmetric cusps; a cusp profile having the correct functional form must be employed in fitting. In addition, the use of multiple, independent methods of determining the beam velocity (see Ref. [13], for example) is very desirable.

ACKNOWLEDGMENTS

We wish to thank N. L. Jones for his able assistance in the operation of the ORNL EN tandem Van de Graaff accelerator. We also wish to acknowledge Dr. C. P. Bhalla and Dr. J. Macek for helpful discussions and Dr. J. Wang and Dr. R. E. Olson for making their CTMC calculations available. This research is sponsored by U.S. Department of Energy, Office of Basic Energy Sciences, Division of Chemical Sciences, under Contract No. DE-AC05-84OR21400 with Martin Marietta Energy Systems, Inc. and by the Oak Ridge National Laboratory Postdoctoral Research Associates Program (J.M.S. and J.L.S) administered jointly by the Oak Ridge Institute for Science and Education and Oak Ridge National Laboratory.

[1] N. Stolterfoht, D. Schneider, D. Burch, H. Wieman, and J. S. Risley, Phys. Rev. Lett. **33**, 59 (1974).
[2] C. Dal Cappello, C. Tavard, and A. Lahmam-Bennani, Phys. Rev. A **26**, 2249 (1982).
[3] F. Bell, H. Böckl, M. Z. Wu, and H.-D. Betz, J. Phys. B **16**, 187 (1983).
[4] D. H. Lee, P. Richard, T. J. M. Zouros, J. M. Sanders, J. L. Shinpaugh, and H. Hidmi, Phys. Rev. A **41**, 4816 (1990).
[5] H. Böckl and F. Bell, Phys. Rev. A **28**, 3207 (1983).
[6] J. O. P. Pedersen, P. Hvelplund. A. G. Petersen, and P. D. Fainstein, J. Phys. B **23**, L597 (1990).
[7] J. O. P. Pedersen, P. Hvelplund. A. G. Petersen, and P. D. Fainstein, J. Phys. B **24**, 4001 (1991).
[8] A. D. González, P. Dahl, P. Hvelplund, and P. D. Fainstein, J. Phys. B **26**, L135 (1993).
[9] H. I. Hidmi, P. Richard, J. M. Sanders, and T. J. M. Zouros, in *VIth International Conference on the Physics of Highly Charged Ions*, edited by P. Richard, M. Stöckli, C. L. Cocke, and C. D. Lin, AIP Conf. Proc. No. 274 (AIP, New York, 1993), pp. 319–322.
[10] H. I. Hidmi, P. Richard, J. M. Sanders, H. Schöne, J. P. Giese, D. H. Lee, T. J. M. Zouros, and S. L. Varghese, Phys. Rev. A **48**, 4421 (1993).
[11] W. Wolff, H. E. Wolf, J. L. Shinpaugh, J. Wang, R. E. Olson, P. D. Fainstein, S. Lencinas, U. Bechthold, R. Hermann, and H. Schmidt-Böcking, J. Phys. B **26**, 4169 (1993).
[12] J. L. Shinpaugh, W. Wolff, H. E. Wolf, U. Ramm, O. Jagutzki, H. Schmidt-Böcking, J. Wang, and R. E. Olson. J. Phys. B **26**, 2869 (1993).
[13] J. H. Posthumus, N. Glargaard, J. N. Madsen, L. H. Andersen, P. Hvelplund, and K. Taulbjerg, J. Phys. B **27**, 2521 (1994).
[14] P. D. Fainstein, V. H. Ponce, and R. D. Rivarola, Phys. Rev. A **45**, 6417 (1992).
[15] J. Wang, C. O. Reinhold, and J. Burgdörfer, Phys. Rev. A **44**, 7243 (1991).
[16] D. Burch, H. Wieman, and W. B. Ingalls, Phys. Rev. Lett. **30**, 823 (1973).
[17] J. S. Lee, J. Chem. Phys. **66**, 4906 (1977).
[18] R. Mann, S. Hagmann, and L. Weitzel, Nucl. Instrum. Meth-

ods Phys. Res. B **34**, 403 (1988).
[19] S. D. Berry, G. A. Glass, I. A. Sellin, K.-O. Groeneveld, D. Hofmann, L. H. Andersen, M. Breinig, S. B. Elston, P. Engar, and M. M. Schauer, Phys. Rev. A **31**, 1392 (1985).
[20] P. R. Bevington, *Data Reduction and Error Analysis for the Physical Sciences* (McGraw-Hill, New York, 1969).
[21] W. Meckbach, I. B. Nemirovsky, and C. R. Garibotti, Phys. Rev. A **24**, 1793 (1981).
[22] J. Wang and R. E. Olson (private communication).